RESEARCH ARTICLE

The Role of Cellular Coupling in the Spontaneous Generation of Electrical Activity in Uterine Tissue

Jinshan Xu[1], Shakti N. Menon[2], Rajeev Singh[2], Nicolas B. Garnier[3], Sitabhra Sinha[2], Alain Pumir[3,4]*

1 College of Computer Science, Zhejiang University of Technology, Hangzhou, China, 2 The Institute of Mathematical Sciences, CIT Campus, Taramani, Chennai 600113, India, 3 Laboratoire de Physique, Ecole Normale Supérieure de Lyon, F-69007, Lyon, France, 4 Max-Planck Institute for Dynamics and Self-Organisation, D-37073, Göttingen, Germany

* alain.pumir@ens-lyon.fr

Abstract

The spontaneous emergence of contraction-inducing electrical activity in the uterus at the beginning of labor remains poorly understood, partly due to the seemingly contradictory observation that isolated uterine cells are not spontaneously active. It is known, however, that the expression of gap junctions increases dramatically in the approach to parturition, by more than one order of magnitude, which results in a significant increase in inter-cellular electrical coupling. In this paper, we build upon previous studies of the activity of electrically excitable smooth muscle cells (myocytes) and investigate the mechanism through which the coupling of these cells to electrically passive cells results in the generation of spontaneous activity in the uterus. Using a recently developed, realistic model of uterine muscle cell dynamics, we investigate a system consisting of a myocyte coupled to passive cells. We then extend our analysis to a simple two-dimensional lattice model of the tissue, with each myocyte being coupled to its neighbors, as well as to a random number of passive cells. We observe that different dynamical regimes can be observed over a range of gap junction conductances: at low coupling strength, corresponding to values measured long before delivery, the activity is confined to cell clusters, while the activity for high coupling, compatible with values measured shortly before delivery, may spread across the entire tissue. Additionally, we find that the system supports the spontaneous generation of spiral wave activity. Our results are both qualitatively and quantitatively consistent with observations from *in vitro* experiments. In particular, we demonstrate that the increase in inter-cellular electrical coupling observed experimentally strongly facilitates the appearance of spontaneous action potentials that may eventually lead to parturition.

Introduction

It is well known that the contraction of uterine smooth muscle cells (myocytes) is triggered by electrical activity resulting from action potentials that evolve from single spikes to spike trains in the lead up to parturition [1–3]. However, the precise mechanism underlying the transition of the uterus from the quiescent organ seen during most stages of pregnancy, to the rhythmically contracting muscle observed at the onset of labor, remains to be fully explained. Preterm births, which occur prior to 37 weeks of gestation, can spontaneously arise from early, undesired uterine contractions [4], and hence this process is highly significant from a clinical perspective. Indeed, recent data suggests that preterm births constitute approximately 10% of all births [5], and that rates of spontaneous preterm labor have been increasing at the same rate as elective or induced preterm births [6]. Preterm births have been implicated as the cause of over a million neonatal deaths per year worldwide, and in around 50% of all cases of infant neurological damage [4]. In the USA alone, they have been linked to 40% of all infant deaths [7]. A clearer understanding of the mechanism of spontaneous uterine tissue contraction could therefore greatly facilitate the development of effective strategies to help curb neonatal mortality and morbidity.

It has been postulated that spontaneous electrical oscillations in human uterine tissue, observed prior to the mechanical contractions of the pregnant uterus, may be initiated by "pacemaker" cells [8, 9], similar to the Interstitial cells of Cajal, which are known to act as a pacemaker in other smooth muscles, such as the rabbit urethra [10, 11]. However, despite much effort aimed at identifying the origin of spontaneous uterine contractions [12], there has thus far been no clear evidence for the existence of such cells in the human uterus. On the contrary, uterine tissue is known to contain an abundance of electrically passive cells, such as Interstitial Cajal-like Cells (ICLCs) or telocytes [13] which, despite their similarity to Cajal cells, have been argued to inhibit electrical activity [11, 14]. ICLCs have a density of about $100 - 150$ cells/mm^2 in the uterus, and contribute up to $\sim 18\%$ of the cell population immediately below the mucosal epithelium [14, 15]. Their density is highest on the surface of the uterus and decreases to a value of around 7.5% in muscularis [14]. Other electrically passive uterine cells include fibroblasts [14], which play an important role in remodeling the human uterine cervix during pregnancy and parturition [16, 17].

The hypothesis that spontaneous electrical behavior is an inherent property of uterine smooth-muscle cells [8] has gained traction as it is known that numerous electrophysiological changes occur in the myometrium during the course of pregnancy. In human uterine tissue, the myocyte resting potential has been observed to change from a value close to $-70mV$ at the beginning of pregnancy to around $-55mV$ at midterm [18]. These changes can be related to the morphological modulations of the uterine tissue [3], that are particularly apparent shortly before delivery. As the tissue enlarges to accommodate the growing fetus, its weight increases from around 75g to 1300g in humans [19]. However, it has not yet been demonstrated that such changes are responsible for the spontaneous generation of action potentials necessary for the periodic mechanical contractions of the uterine tissue [19].

Studies on rats uterine tissue generally corroborate the picture obtained in the human uterus. In particular, the results of [20] do not reveal the presence of any pacemaker cells. The changes in the outward (K$^+$) and inward (Na$^+$, as well as Ca^{2+}) currents have been documented [21, 22]. It has been observed from experiments on rat uterine myocytes that the recorded peak current in the Na$^+$ channel increases from $\sim 2.8\mu A/cm^2$ in a non-pregnant uterus to $\sim 5.1\mu A/cm^2$ at late pregnancy, while the corresponding peak current in the Ca^{2+} channel decreases from $\sim 5.7\mu A/cm^2$ to $\sim 3.4\mu A/cm^2$ over the same range [21]. These changes are accompanied by changes in both the surface area of a single myocyte cell, from $\sim 1930\mu m^2$

to $\sim 7600 \mu m^2$ during late pregnancy, and, consistent with the observed hypertrophy of the uterus, a five-fold increase in the cell capacitance [21].

In rat uterine tissue, an alternative paradigm for the genesis of coherent uterine activity is hinted at by the fact that an even more dramatic change occurs close to term in the uterus. The fractional area of gap junctions, defined as the ratio of the membrane area occupied by gap junctions to the total membrane area, has been observed to show a 20-fold increase in the rat uterus [23]. Furthermore, the gap junctional conductance has been found to increase from ~ 4.7 nS at normal preterm to ~ 32 nS during delivery [24], while a reduced expression of the major gap junction protein connexin 43 in transgenic mice is known to significantly delay parturition [25]. It is well-known that the electrical coupling by gap junctions affects the conduction velocity of waves of activity propagating through the tissue: propagation in cardiac tissue is only possible when the coupling is strong enough, and the velocity of propagation increases with the coupling strength, i.e., the gap junction expression [26]. The importance of gap junction expression is manifested most spectacularly in the observation that chemical disruption of the gap junctions immediately inhibits the oscillatory uterine contractions [27–29]. These findings strongly suggest that gap junctional coupling between proximate cells plays a very important role in the development of coordinated uterine electrophysiological activity, and may be responsible for the transition from the weak, desynchronized myometrial contractions seen in a quiescent uterus to the strong, synchronous contractions observed during labor [23, 24].

It has recently been observed that the coupling of an excitable cell to an electrically passive cell in a simple theoretical model of myocyte activity can give rise to oscillations, even if neither of the cells are initially oscillating [30]. This prediction seems to be borne out by experiments, as the coupling of electrically active and passive cells in an assembly is indeed known to significantly affect the observed synchronization dynamics [31, 32], while complicated dynamical regimes are observed in preparations of weakly coupled cardiac myocytes [33, 34]. The physiological significance of this phenomenon can be inferred from the fact that the activity synchronizes at high coupling strengths in both experimental preparations and numerical simulations of theoretical models. This synchronization first occurs over small regions (cell clusters) whose size gradually increases to fill out the full media, so that all cells beat with the same frequency [31, 35, 36].

Consequently, it has been hypothesized [36] that spontaneous oscillatory behavior could be initiated by the strong increase in coupling between non-oscillating electrically active and passive cells of a pregnant uterus shortly before delivery. Further justification for this claim stems from the fact that in rat uterine tissue, close contact between ICLCs and smooth muscle cells has been observed [20]. Moreover, while there has thus far been no direct evidence for the electrical coupling between myocytes and fibroblasts via gap junctions, analogous *in vitro* studies of rats [37] or rabbits [38] cardiac tissue strongly suggest the occurrence of such coupling. The resting potential of ICLCs, V_I^r is around $V_I^r \sim -58 \pm 7mV$ [20] and, while the resting potential of fibroblasts, V_F^r, varies over a large range (-70 mV to 0 mV), it is mostly in the range $-25mV \leq V_F^r \leq 0mV$ (in 77.3% of all cases), with a peak of the distribution at $-15mV$ [39]. As both cells have resting potentials larger than that of the myocyte, they can act as a source of depolarizing current on coupling, and are thus potentially significant participants in the generation of spontaneous activity [30, 36]. However, the argument that spontaneous uterine activity is a result of coupling between electrically active and passive cells has thus far been tested only on a highly simplified model of myocyte electrical activity [36], and no significant attempt has yet been made to relate the model parameters to actual observations.

Recently developed realistic, biologically detailed models of uterine myocytes [40, 41] allow for a precise theoretical study of the roles of individual physiological components in the

generation of desirable, as well as pathological, electrical activity, which in turn permits a better understanding of their correlation with contractile force [42, 43]. The purpose of the present work is to investigate the effect of cell coupling on spontaneous electrically activity using an electrophysiologically realistic mathematical model, and to examine the synchronization behaviour that occurs when this coupling is sufficiently strong. To this end, we present a model for the electrical activity of uterine smooth muscle cells coupled to passive cells. This model is based on a realistic mathematical description of rat uterine smooth muscle cell electrical activity recently developed by Tong *et al.* [41], which uses a general Hodgkin-Huxley formalism to describe the evolution of the membrane potential of myocytes, V_m, and the Calcium ionic concentration in the cytosol, $[Ca^{2+}]_i$. The details of our model are discussed in the Methods section. The most significant modification we make to the model of Tong *et al.* is the addition of an extra current, arising from the electrical coupling, and an associated equation for the evolution of the passive cell potential.

In the following section, we present the results of a systematic investigation into the conditions that give rise to spontaneous electrical activity, in particular the dependence of myocyte activity on gap junction conductivity, passive cell resting potential and the number of passive cells. Furthermore, we examine the regimes that arise when myocytes and passive cells are coupled in a two-dimensional (2-D) assembly. This 2-D configuration mimics a cell culture of the type routinely used in cardiac preparations [33, 34], or in experiments performed on the pregnant uteri of small animals [44], thus facilitating the potential experimental verification of our observations. Our numerical results strongly suggest that coupling plays an important role in both the appearance of oscillations as well as in the emergence of synchronized activity in the tissue. Moreover, we find that our model is capable of capturing rich dynamical regimes, characterized by periodically spaced, irregular patterns of action potentials, that are qualitatively consistent with recent observations [44].

Materials and methods

Our mathematical model builds upon the description of rat uterine smooth muscle cell activity developed by Tong *et al.* [41], which consists of a set of first order ordinary differential equations that describe the evolution of fourteen ionic currents, including depolarizing Na$^+$ and Ca^{2+} currents and repolarizing K$^+$ currents. The description of each ionic current involves activating and inactivating gating variables, m_h which specify the state of each channel h, and are governed by evolution equations of the type:

$$\frac{\mathrm{d}m_h}{\mathrm{d}t} = \frac{m_h^\infty - m_h}{\tau_h} , \qquad (1)$$

where $m_h^\infty (= \alpha_h/(\alpha_h + \beta_h))$ are the asymptotic values of m_h, $\tau_h (= 1/(\alpha_h + \beta_h))$ are the relaxation times, and α_h (β_h) are the rates at which the channels open (close). The relaxation times are represented by nontrivial functions of the membrane potential, V_m, that are typically determined experimentally.

We describe the excitation dynamics of myocytes in terms of the time evolution of this membrane potential:

$$C_m \frac{\mathrm{d}V_m}{\mathrm{d}t} = -I_{\mathrm{ion}} + I_{\mathrm{ext}} + I_{\mathrm{gap}} , \qquad (2)$$

where C_m is the cell membrane capacitance, I_{ion} is the sum of the fourteen trans-membrane ionic currents and I_{ext} accounts for any externally applied current. This expression differs from that used in the model by Tong *et al.* [41] in that we include an additional gap-junction

mediated coupling current, I_{gap}. This term accounts for the current I_{gap}^p induced by the interaction of myocytes with passive cells and, in the case of a 2-D lattice, the additional inter-myocyte coupling current I_{gap}^m. We use the standard convention where outward ionic currents and externally applied currents are taken as positive. For the purposes of the present study, we ignore the effect of external currents and set $I_{\text{ext}} = 0$.

The model by Tong *et al.* [41] also describes the evolution of the intra-cellular Calcium ion concentration, $[\text{Ca}^{2+}]_i$, in the cytosol,

$$\frac{\text{d}[\text{Ca}^{2+}]_i}{\text{d}t} = -\left(J_{\text{Ca,mem}} + J_{\text{PMCA}} + J_{\text{NaCa}}\right),\qquad(3)$$

where the flux of Calcium ions has three components: (i) $J_{\text{Ca,mem}}$, which represents Calcium flux from specific membrane channels, including L and T-types and other nonspecific cation currents; (ii) J_{PMCA}, which represents the flux of plasmalemmal Ca^{2+}-ATPase; and (iii) J_{NaCa}, which represents flux from Na^+-Ca^{2+} exchangers. The currents resulting from the plasmalemma and from the exchangers both extrude Calcium ions from the cell. In particular, the Na^+-Ca^{2+} exchangers extract one Ca^{2+} ion from the cytosol for three Na^+ ions pumped into the cell [45]. By their very nature, the ionic currents J_{PMCA} and J_{NaCa} must extrude Calcium, and as such, must be positive. Consequently, the current resulting from the action of the exchanger, I_{NaCa}, is inward (or repolarizing) and hence, by the standard convention, negative. In our model we have ensured that the known physiological functions of the exchangers are cogently described, and that the requirements that $J_{\text{NaCa}} \geq 0$ and $I_{\text{NaCa}} \leq 0$ are satisfied. Additionally, motivated by the experimental literature (in particular [45]) as discussed in Sec. S.2 of the SI, we used different parameter values for the terms that describe the Na^+-Ca^{2+} exchanger.

In order to motivate the electrical coupling mediated by gap junctions between myocytes and passive cells, we note the observation [20] that although ICLCs do not exhibit regular spontaneous depolarizations and appear unable to generate action potentials, the application of an external current causes their membrane potential to relax at a near-exponential rate with a characteristic time scale of $\sim 0.2 - 1s$ (see Fig. 7B of [20]). Thus, when a passive cell of this type is electrically coupled to a myocyte, its membrane potential dynamics can be described by:

$$C_P \frac{\text{d}V_P}{\text{d}t} = G_P^{\text{int}}(V_P^r - V_P) + I_{\text{gap}}^p,\qquad(4)$$

where C_P, G_P^{int} and V_P^r represent the capacitance, conductance and resting potential, respectively, of a generic passive cell and I_{gap}^p is the coupling current. As a consequence, a myocyte with n_p passive cells in its neighborhood experiences a coupling current $I_{\text{gap}} = -n_p I_{\text{gap}}^p$. The current I_{gap}^p is proportional to the difference between the potentials of the myocyte, V_m, and passive cell, V_P, across the electrically conducting pores that result from the existence of gap junctions. The coupling-induced current can hence be expressed as $I_{\text{gap}}^p = G_p (V_m - V_P)$, where the gap junction conductance, G_p, is directly related to the level of expression of the connexin proteins that constitute these junctions. As the conductance of a single gap junction channel has been estimated to be of the order of 50 pS [46], the relation between the conductance and then number of expressed gap junctions n_{gj} is simply $n_{gj} \approx G_p/50$ pS.

We note that although Eq. (4) is sufficient for our current purposes, it does not capture the full complexity of the passive cell membrane dynamics. As seen in Fig. 7B of [20], when the applied current is varied, the relaxation time scale changes, suggesting a dependence of G_P^{int} as a function of the membrane potential. We further note that although Eq. (4) was formulated based on known properties of ICLCs, it can also be used to describe the behaviour of other electrically passive cells, such as fibroblasts, which have a membrane conductance of $G_F^{\text{int}} = 1nS$

[47]. Indeed, it is instructive to consider the case where myocytes are simultaneously coupled to different types of passive cells (see Sec. S4 of the SI for more details).

In order to describe the effect of inter-myocyte coupling, we assume that myocytes are coupled to their nearest neighbors on a 2-D square lattice of size $N \times N$, and label each cell by the indices of its row (a) and column (b). In this case, each myocyte receives a coupling current I_{gap}^m given by

$$I_{\text{gap}}^m(a, b) = G_m(V_m(a+1, b) + V_m(a-1, b) + V_m(a, b+1) + V_m(a, b-1) - 4V_m(a, b)), \quad (5)$$

where G_m is the conductance of the myocyte gap junctions. The total coupling current experienced by a myocyte coupled to both electrically passive cells, as well as other myocyte cells in a lattice (see Fig. 1) is thus $I_{\text{gap}} = -n_p I_{\text{gap}}^p + I_{\text{gap}}^m$. The coupling current Eq. (5) has the form of a diffusive term, with G_m/C_m acting as an effective diffusion constant. We note that in the simple lattice, represented in Fig. 1, the distance between adjacent cells is expected to be of the size of the individual myocytes, which are known to be of the order of $100\mu m$. In view of the very anisotropic shape of the cells [21], however, it is difficult to establish a very precise correspondence between the intercellular distance in the model and realistic properties of the tissue. This limitation does not affect the qualitative conclusions of the present work.

Finally, we note that one of the relaxation times τ_α can be of the order of several hundred pico seconds, and hence, the maximum simulation time step is greatly constrained. However, this very short time scale implies that the gating variable x_α relaxes very quickly to its steady-state value. Thus, in order to increase numerical efficiency, we make the assumption that $x_\alpha(t) = x_{\alpha\infty}(V_m)$, which allows us to use a comparatively larger time step $dt = 0.5ms$. We have verified that the numerical results are not sensitive to this approximation, with only a 0.25% error in the periods of oscillation.

Apart from the details described above, our model equations and the parameter values used in our simulations correspond exactly to those used in Ref. [41]. Our numerical simulations involved the integration of the set of ordinary differential equations using a standard fourth-order Runge-Kutta scheme. For improved efficiency, the Message-Passing-Interface (MPI) library was implemented to distribute the load among up to 16 processors. When obtaining time series data, care was taken to ensure that any transient behaviour was discarded. While our model behaves slightly differently from the model by Tong *et al.* [41] in response to external stimuli (see Sec. S.3.2 of the SI), we emphasize that, as in Ref. [41], results obtained using our model are consistent with data from voltage clamp experiments (see Sec. S.3.1 of the SI for details of our validation tests). In addition, we have verified that our results are qualitatively robust, by simulating both the single cell and 2-D cases with slightly different sets of parameters, different realizations and, in the 2-D case, a larger lattice. We note that for a sufficiently large lattice size, the results do not qualitatively depend on N.

Results

We now investigate the hypothesis mentioned in the introduction, namely that the interaction between coupled myocytes and passive cells is fundamental to their spontaneous activation during the late stages of pregnancy. As the number of gap junctions are known to increase during this period [24], one expects higher values for the effective coupling conductances G_p and G_m. Moreover, although individual passive cell types are each characterized by a unique resting potential, a mixture of passive cell types can result in an effective V_p^r that is different from those of the constituent cells. The effect of such phenomena on the dynamical behavior of the coupled system are shown below. In the following subsections, we present a numerical investigation of the electrical activity of myocyte cells coupled to n_p passive cells, followed by a study of
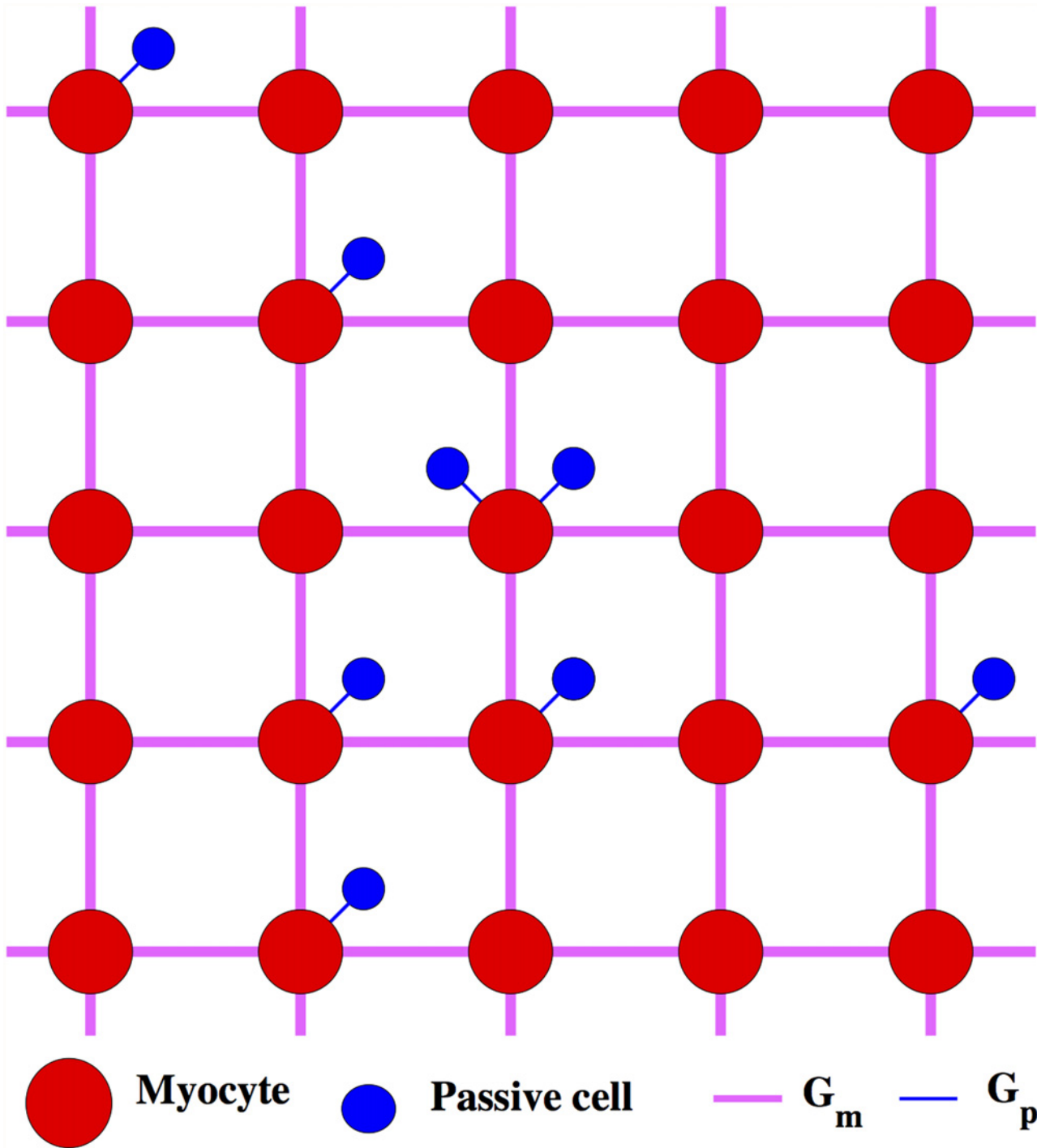
Fig 1. Schematic representation of the 2-D tissue. Schematic representation of the 2-D square lattice of uterine myocytes (shown in red), each myocyte coupled to a random number of passive cells (shown in blue). Neighboring myocytes are electrically coupled with strength G_m and the coupling strength between a myocyte and a passive cell is G_p.

the emergence of regimes of regular and irregular dynamical activity in a 2-D lattice of myocytes coupled to each other, as well as to passive cells.

3.1 Coupling a single myocyte to electrically passive cells

A myocyte is known to exhibit oscillatory behaviour when external current is injected into it (see SI for more details). As coupling through gap junctions with neighboring cells provides a source of such an inward current, the electrical state of a myocyte coupled to passive cells can be dynamically modulated by changing the strength of this coupling. When neighboring myocytes in a tissue are strongly coupled, as would be expected towards the late stages of pregnancy [24], their behaviour is sensitive to the average number of passive cells in the tissue—a property that we have explicitly verified through numerical simulations on an assembly of cells [48]. The limiting case of large coupling between myocytes can be approximated by considering a single myocyte coupled to n_p passive cells. Note that as n_p in this case effectively corresponds to the average number of passive cells in the tissue, it can take non-integer values. In the following, we investigate the dependence of the myocyte behaviour on the conductance of gap junctions between myocytes and passive cells, G_p, the passive cell resting potential, V_p^r, and the average number of passive cells coupled to a myocyte, n_p.

In our simulations, we have assumed that the myocyte membrane capacitance is $C_m = 120pF$ and the passive cell has capacitance $C_P = 80pF$ and conductance $G_P^{\mathrm{int}} = 1.0nS$. This is motivated by observations that the capacitance of rat myocytes is around $120pF$ during the late stages of pregnancy [21], and that the capacitance and input resistance of an ICLC are 84.8 ± 18.1pF and 3.04 ± 0.5$G\Omega$, respectively [20]. Additionally, we assume that the sodium conductance is $g_{Na} = 0.04nS/pF$, which is in the range of values measured during late pregnancy (see [41] and references therein). We have verified that our results are robust with respect to small changes in the system parameters.

3.1.1 Dependence on the gap junction conductance. The evolution of the membrane potential of a myocyte, V_m, coupled to a single passive cell is displayed in Fig. 2 for different values of the gap junction conductance, G_p. For values of G_p less than a critical threshold $G_0 \approx 0.164nS$, V_m approaches a steady state, while for values of $G_p > G_0$, the electrical coupling induces spontaneous temporal oscillations whose time period decreases as G_p increases. As seen in Fig. 2a, the oscillation time period for $G_p = 0.1741nS$ is $T \sim 1$ min, while for $G_p = 0.5nS$, we find $T \sim 12s$ (Fig. 2b), and for $G_p = 1nS$, we find $T \sim 7s$ (Fig. 2c). As shown in Fig. 2c, the oscillatory behaviour can be suppressed immediately upon uncoupling the myocyte and the passive cell, i.e., by setting G_p to 0. This is consistent with the experimental observation that the addition of a gap junction uncoupler leads to rapid termination of electrical activity [27]. As G_p approaches G_0 from above, the time period T grows like $T \sim \log[(G_p - G_0)/G_0]$ (see Fig. 2d). Although this logarithmic divergence of time periods close to a critical point is suggestive of a homoclinic bifurcation [49], we note that the dynamical behaviour in the interface between the regimes of activity and inactivity is in fact more complicated. We observe that there exists a small range of values of G_p for which both stable and oscillatory solutions are possible. Depending on the precise choice of initial condition, the system may evolve to either of the two asymptotic solutions (attractors), corresponding to quiescence or oscillations.

3.1.2 Dependence on the passive cell resting potential. The time periods, T, of the oscillations of the membrane potential, obtained for different values of the passive cell resting potential, V_p^r, and the gap junction conductance, G_p, are displayed in Fig. 3. Consistent with the observations of Fig. 2d, the period of oscillation is very large close to a threshold value of G_p for values of V_p^r larger than $\sim -42mV$. In addition, T increases on decreasing V_p^r. For any given G_p, there exists a threshold value of V_p^r below which the solution approaches a steady, non-
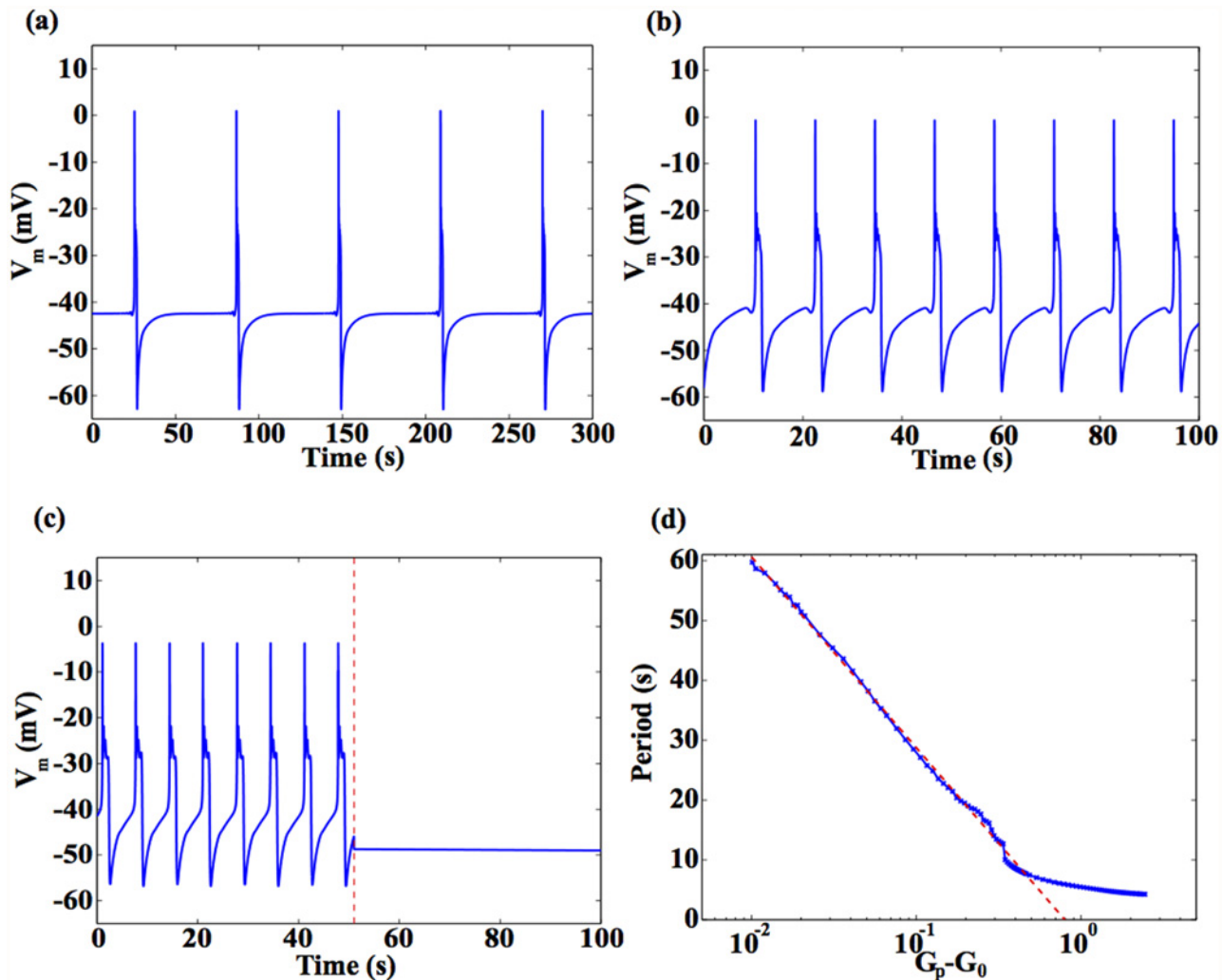
Fig 2. Possible dynamical regimes of a myocyte coupled to a passive cell. Dynamical behaviour of a myocyte coupled to a passive cell for different values of the gap junction conductance G_p, and with $V_p^r = -35mV$ and $n_p = 1$. (a) At $G_p = 0.174nS$, the period is $\sim$ 1min. (b) At $G_p = 0.5nS$, the period has reduced to $\sim$ 12s. (c) At $G_p = 1nS$, the period reduces further to $\sim$ 7s. Here we observe that the sudden uncoupling of the myocyte and passive cell, at the time indicated by the vertical broken line, immediately terminates activity. (d) Above a critical value $G_0 = 0.164nS$, we observe a logarithmic divergence in the oscillatory time period: $T \sim \log[(G_p - G_0)/G_0]$ as indicated by the broken line.

oscillating state. Conversely, as V_p^r increases, one finds that T decreases, and can be as low as a few seconds for large values of V_p^r and G_p. As in the situation discussed in the previous subsection, the system can evolve to either a quiescent or oscillatory solution when V_p^r and G_p are close to the bifurcation line (indicated in Fig. 3 by a continuous curve).

Fig. 3 suggests, in particular, that the gap junction conductance threshold is a decreasing function of V_p^r. This can be qualitatively understood by noticing that coupling a myocyte to a passive cell is equivalent to the addition of a current $I_{ext} \sim -\frac{G_p^{int} G_p}{G_p^{int} + G_p} V_p^r$ in the expression for myocyte membrane potential, Eq. (2), at least in the limit of large passive cell relaxation time. From this expression for the external current I_{ext}, elementary algebraic considerations show that as the potential V_p^r increases, the coupling G_p necessary to deliver a given current decreases (see also Supplementary Information).
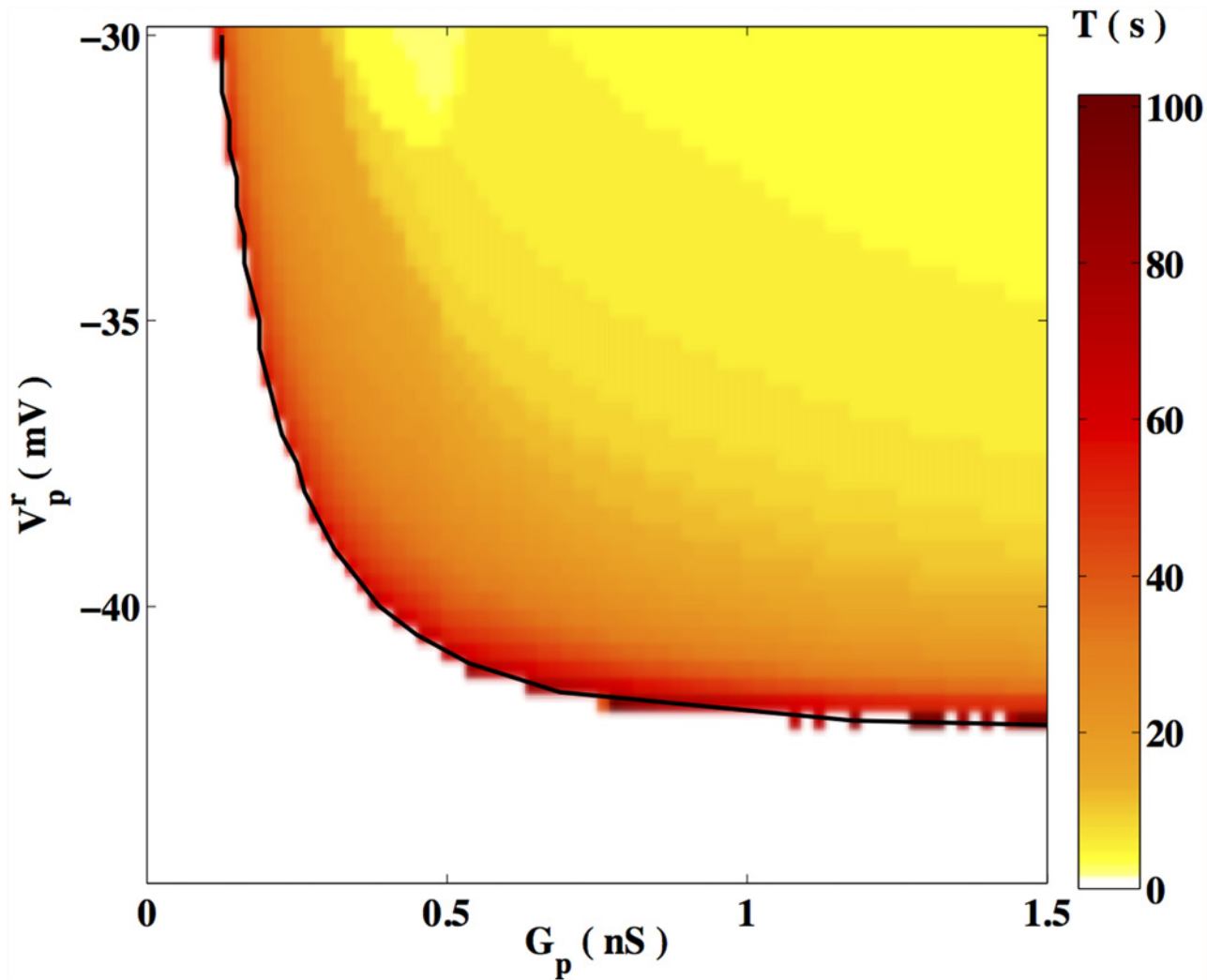
Fig 3. Time periods *T* of the oscillation as a function of coupling. The time period T (in sec) of the membrane potential, for a range of values of V_p^r and G_p. Regions shown in white correspond to the absence of oscillatory activity. The bifurcation from oscillatory activity to a quiescent dynamical regime occurs at the interface indicated by the continuous curve obtained by fitting numerical data.

doi:10.1371/journal.pone.0118443.g003

3.1.3 Dependence on the number of passive cells. It is known that the total number of passive cells in uterine tissue is only a fraction of that of the myocytes [19]. As mentioned earlier, each myocyte is attached to n_p passive cells. Fig. 4 displays the domain of oscillatory activity in the (G_p, n_p) plane, observed for two different choices of the passive cell resting potential: $V_p^r = -40mV$ (Fig. 4a) and $V_p^r = -35mV$ (Fig. 4b). In each case, we find that the cell is quiescent for low values of G_p and n_p, while spontaneous oscillatory activity is generated on increasing these parameters. We note from Fig. 4 that for any given value of G_p there exists a critical value of n_p below which spontaneous oscillations will not occur. In the limit $1/G_p \rightarrow 0$, we find this critical value to be $n_p \approx 0.28$ ($n_p \approx 0.17$) for a passive cell resting potential $V_p^r = -40mV$ ($V_p^r = -35mV$).

We observe that the curve delimiting the region of activity in Fig. 4 has a simple analytic form $n_p = A/G_p + B$, where the parameters A and B are related by $B = A/G_p^{\text{int}}$. In the limit where the passive cell resistivity G_p^{int} is large, the passive cell membrane potential relaxes
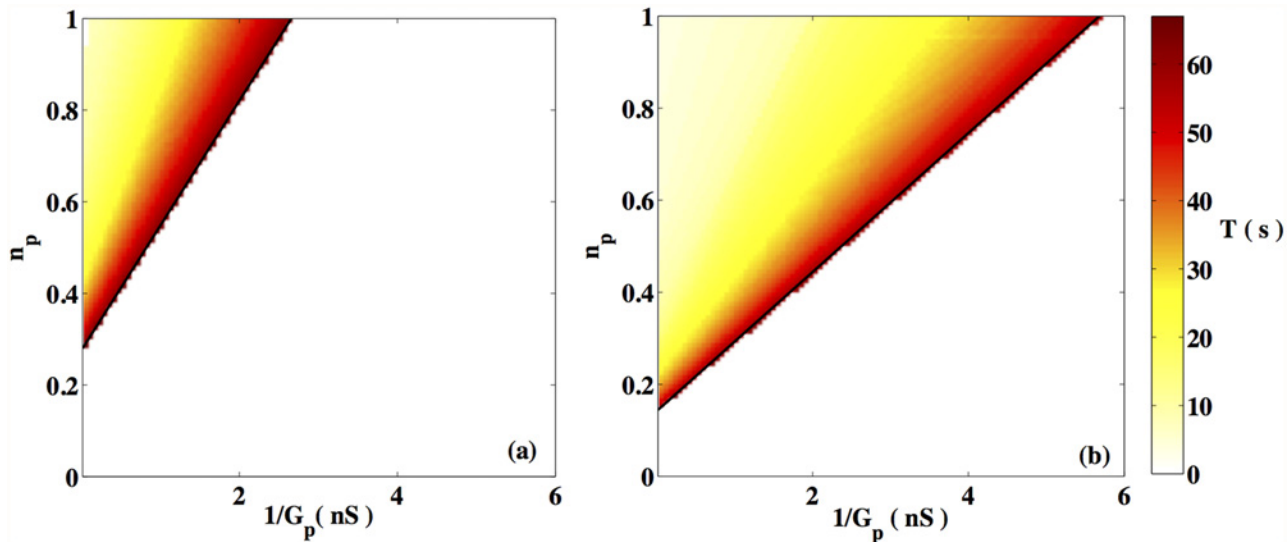
Fig 4. Time periods T as a function of the number of coupled passive cell. Time periods of oscillation, T (in sec) at two different values of V_p^r, for a range of values of n_p and G_p. Regions shown in white correspond to the absence of oscillatory activity. Activity is seen when $n_p \geq A + B/G_p$ (indicated by the solid line), a functional form that can be justified from elementary considerations, see text. (a) $V_p^r = -40mV$ ($A \approx 0.28$, $B \approx 0.27$) (b) $V_p^r = -35mV$ ($A \approx 0.17$, $B \approx 0.15$).

doi:10.1371/journal.pone.0118443.g004

quickly to its equilibrium value. From Eqs. (2) and (4) one can show that the coupling term in Eq. (2) is equivalent to adding an external current $I_{ext} \sim -n_p \frac{G_p^{\text{int}} G_p}{G_p^{\text{int}} + G_p} V_p^r = -n_p / \left(\frac{1}{G_p^{\text{int}}} + \frac{1}{G_p} \right) V_p^r$. This expression implies that the effect of the coupling in the equation for the myocyte action potential depends on the quantity $n_p / \left(\frac{1}{G^{\text{int}p}} + \frac{1}{G_p} \right)$, which is constant provided n_p is proportional to $1/G_p^{\text{int}} + 1/G_p$. Hence the analytical form for n_p stated above delineates the region of parameter space where oscillations occur (Fig. 4).

3.2 Coupling myocytes to passive cells in a 2-D lattice

We now investigate dynamical patterns of activity that arise on a spatially extended domain characterized by nearest-neighbor interactions between the myocytes. To this end, we assume that myocytes are electrically coupled in an $N \times N$ square lattice (Fig. 1); we take $N = 50$ in the present study. Additionally, each myocyte is coupled to an integer number of passive cells n_p drawn from a random distribution $P(n_p)$, chosen here to be binomial with mean $f = < n_p > = 0.2$. Numerical simulations reveal that the precise choice of boundary conditions for our model can affect some qualitative features of the observed patterns. In this paper, we limit our 2-D investigation to the study of the dynamics in an isolated segment of late-pregnant myometrium by imposing no-flux boundary conditions on V_m, thus allowing for direct comparisons with experiments, such as those performed by Lammers and coworkers [44, 50, 51]. In the following, we set $G_p = 3.5nS$ and systematically vary the inter-myocyte gap junction conductance G_m.

3.2.1 Dependence on the inter-myocyte gap junction conductance. The dependence of the electrical activity of the lattice on the inter-myocyte gap junction conductance G_m is shown in Fig. 5. As the coupling strength is known to increase during pregnancy [24], these results are plausibly indicative of the transition towards coherent activity in the uterus close to term.

For low values of G_m, a significant number of cells remain quiescent, while the remaining cells organize themselves into a few localized clusters, each of which are characterized by a
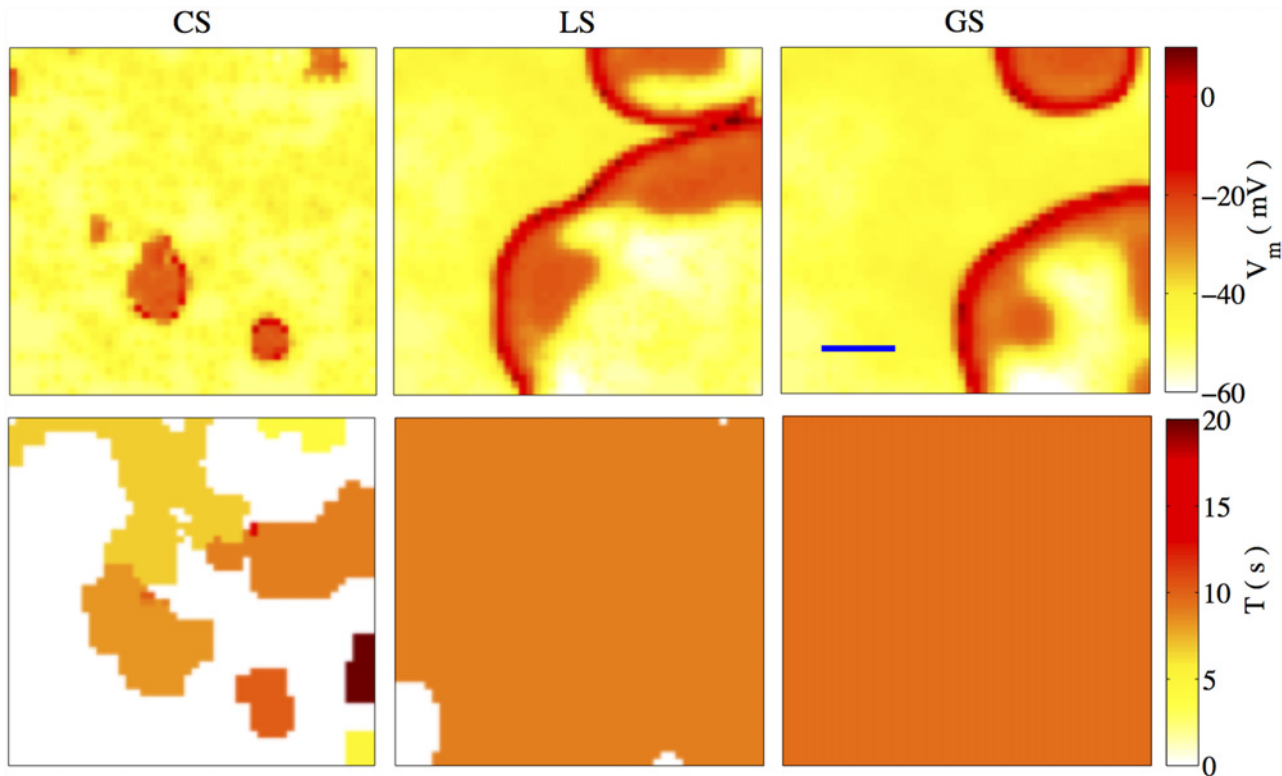
Fig 5. Patterns of electrical activity. Pattern observed for different coupling strengths G_m between myocytes on a 50×50 lattice, where each myocyte interacts on average with $f(= 0.2)$ passive cells. The upper row shows snapshots of the membrane potential while the lower row shows the corresponding effective time periods of oscillatory activity. The horizontal bar in the upper right-most panel indicates the length corresponding to 10 cells, which is of the order of $\sim 1 - 2mm$. (a) Cluster Synchronization (CS) is observed at $G_m = 0.48nS$ where cells group into several synchronously oscillating clusters, each characterized by a different frequency, coexist with regions in which the tissue is at rest. (b) At $G_m = 1.8nS$ all cells in the lattice that oscillate do so with a single frequency. However, we also observe a few non-oscillating cells indicating that this corresponds to the LS regime. (c) At $G_m = 2.4nS$, which lies in the GS regime, every cell in the lattice oscillates with the same frequency.

doi:10.1371/journal.pone.0118443.g005

unique oscillating frequency. This regime, referred to as cluster synchronization (CS), is shown in Fig. 5 (left column), where different clusters with characteristic effective oscillatory periods in the range 5 – 10 sec are observed for $G_m = 0.48nS$. It has been shown, using a simplified model of myocyte activity [48], that the electrical activity originates in regions where the coarse-grained density of passive cells attached to the myocytes is high.

On increasing G_m, we observe that the various clusters begin to merge, eventually giving rise to a scenario where all the cells that oscillate do so with the same frequency (see the middle column of Fig. 5, which displays results for $G_m = 1.8nS$). In this regime, referred to as local synchronization (LS), it is appropriate to define the fraction of oscillating cells, by $n_{osc} = N_{osc}/N^2$ where N_{osc} is the number of oscillating cells [36]. We find the existence of pockets of cells that remain quiescent, and also observe that regions with a high coarse-grained density of passive cells produce travelling waves that propagate through the system, thus effectively acting as "pacemaker regions" [48].

As we increase G_m further, we find that every cell in the system oscillates at exactly the same frequency (see the right column of Fig. 5, which displays results for $G_m = 2.4nS$). This dynamical state is known as global synchronization (GS). The transition from LS to GS is characterized by an increase in the fraction of oscillating cells n_{osc} to 1.
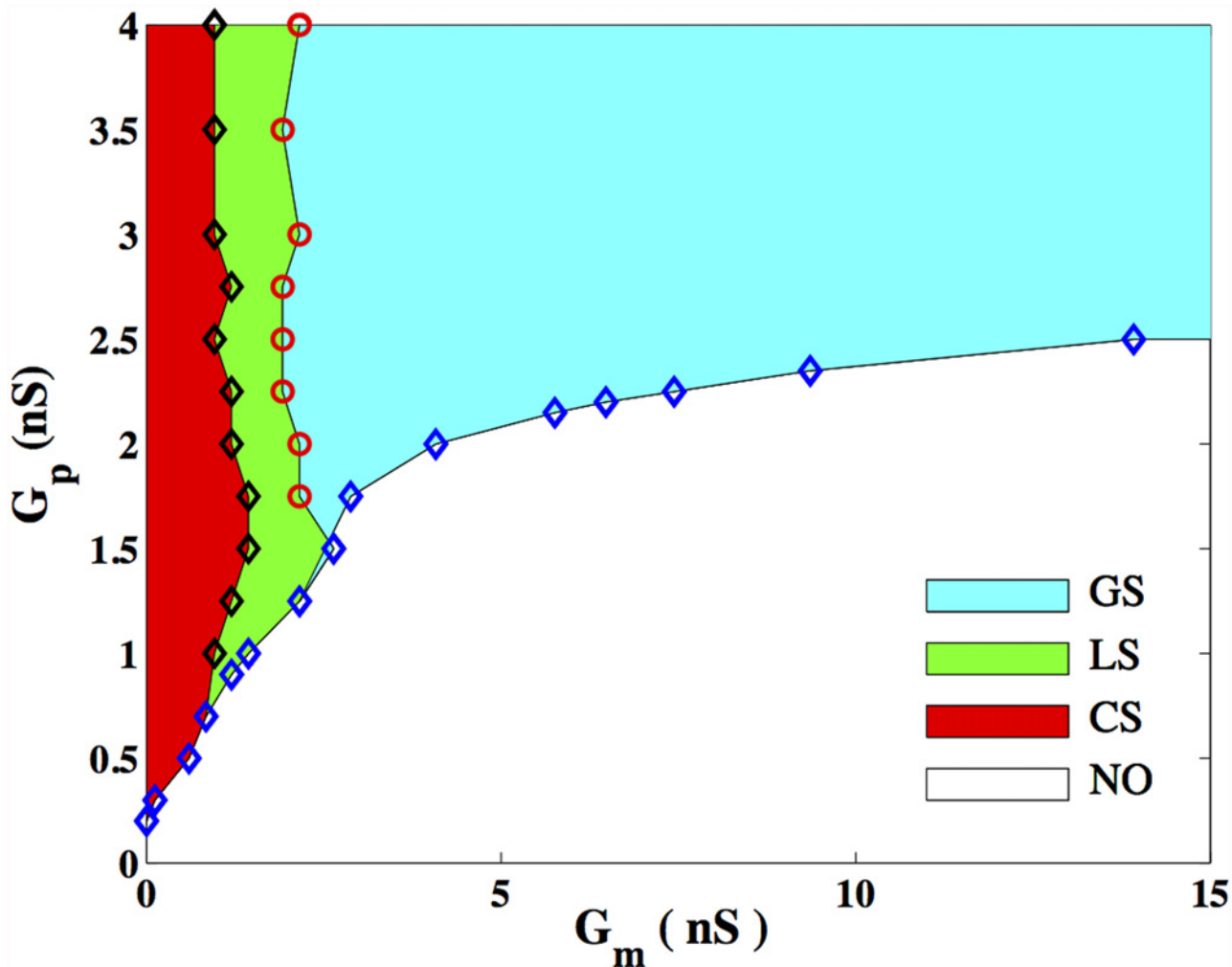
Fig 6. Phase space describing the dynamical systems of the model. Dynamical regimes observed in the 2-D lattice of coupled myocytes and passive cells for a range of coupling strengths. Three distinct synchronization regimes are observed: CS at low G_m, LS at intermediate G_m and GS at high G_m. For every value of G_m, there exists a critical value of G_p below which no oscillations (NO) are observed. The symbols indicate numerically determined points lying on the boundaries between the various dynamical regimes.

doi:10.1371/journal.pone.0118443.g006

The phase diagram in Fig. 6, obtained over a range of values of G_m and G_p, displays the aforementioned regimes of dynamical behaviour, viz., CS, LS and GS. An additional state is seen for sufficiently low G_p and sufficiently large G_m where no oscillations (NO) are observed. We observe in Fig. 6 that when G_m is large, the transition between NO and GS occurs at a value of $G_p \approx 2.7nS$, consistent with Fig. 4. The phase diagram in Fig. 6 is qualitatively similar to that obtained with the simpler FitzHugh-Nagumo model, used for describing the dynamics of an excitable cell [36]. We note that for a range of parameter values in the domain corresponding to GS in Fig. 6, the activity is in fact irregular, an issue discussed in Sec. 3.2.2.

For a sufficiently large inter-myocyte gap junction conductance ($G_m \gtrsim 19.2nS$) the activity of the system is characterized by a simple, regular spatial pattern (Fig. 7). Here, an action potential is emitted in the form of a target wave from a single, dominant region of high passive cell density, which effectively acts as a local pacemaker. The nature of the transition from distinct, competing wave sources at low G_m to a single dominant source at large G_m is explicated
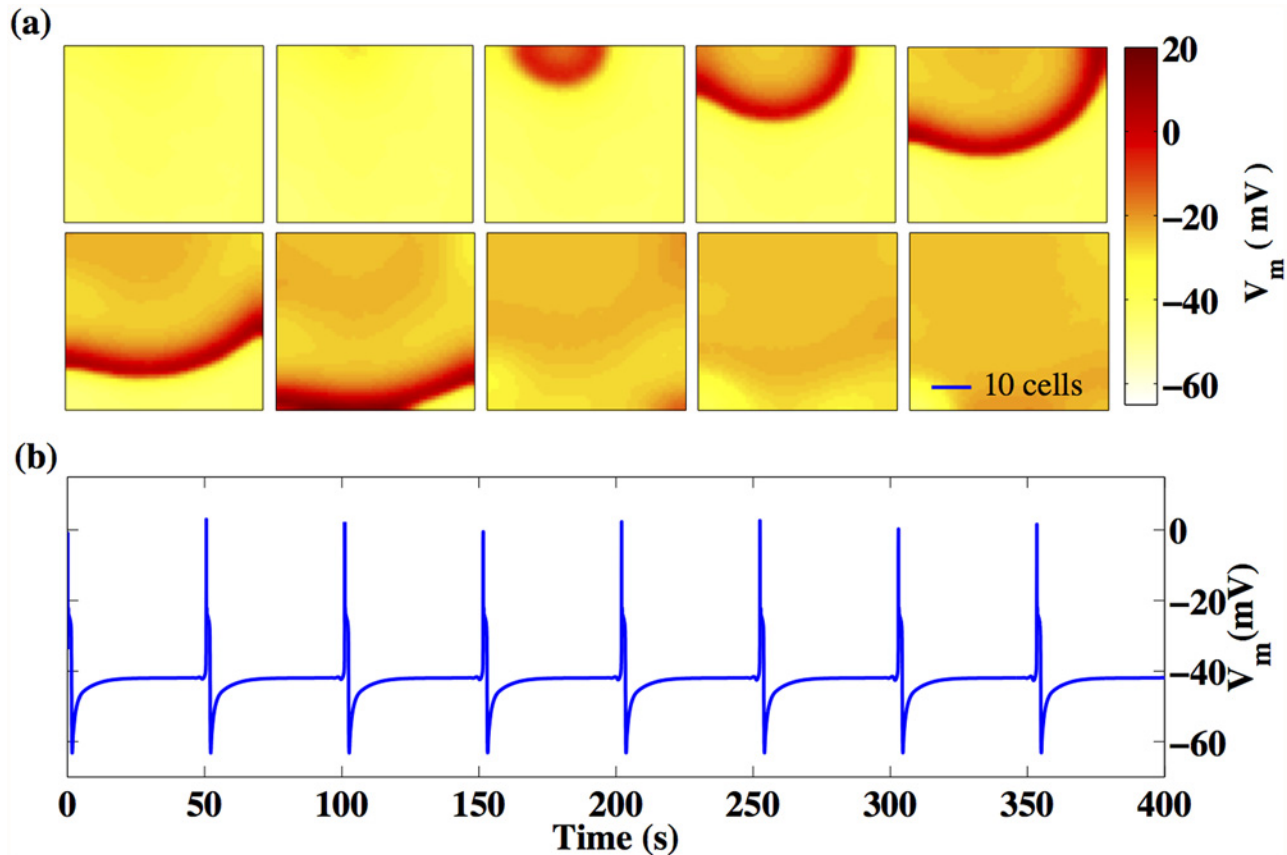
Fig 7. Regular periodic activity in the 2-D lattice of coupled myocytes and passive cells. The regime presented here corresponds to an inter-myocyte coupling strength, $G_m = 20nS$. (a) Waves are emitted periodically from a single, dominant region characterized by high passive cell density. The snapshots are separated in time by 75 ms. The horizontal bar in the lowest, right-most panel indicates the length corresponding to 10 cells, which is of the order of $\sim 1 - 2mm$. (b) This behaviour causes each cell in the system to exhibit a periodic pattern of activity with a period $T \sim 50$ s. The only difference between the recorded time series of any two cells in the system is a temporal shift, dependent on the proximity of the cell to the source.

doi:10.1371/journal.pone.0118443.g007

in Ref. [48]. The range of values of G_m spanned in Fig. 6 correspond to experimentally relevant values of inter-cellular coupling in the uterine myometrium [24]. Based on the results of Ref. [36], we expect that coherent activity over the entire system will be observed at even larger values of G_m.

3.2.2 Emergence of irregular activity. Despite the fact that the activity of all oscillating cells in the LS and GS regimes have the same effective time period, we note that this does not imply that the activity of all cells are temporally synchronized in these regimes, nor that they exhibit simple dynamical behaviour. In fact, for values of the inter-myocyte gap junction conductance in the range $6nS \lesssim G_m \lesssim 19.2nS$ the region of parameter space characterized by GS occasionally exhibits irregular activity: oscillations with a period of $\sim 15s$ that are erratically interrupted, for short durations, by oscillations with a period of $\sim 1s$. This activity arises due to the competition between strong and weak pacemaker-like regions that can, on occasion, generate disordered activity in the form of transient spiral waves. The strength and number of pacemaker-like regions is strongly correlated to the passive cell distribution on the lattice, and the possibility of competition between regions is more significant for larger lattices [48].

As this irregular behaviour occurs in the GS regime, all cells exhibit the same qualitative time series, with only a temporal shift. Hence, we restrict our attention to the behaviour of a
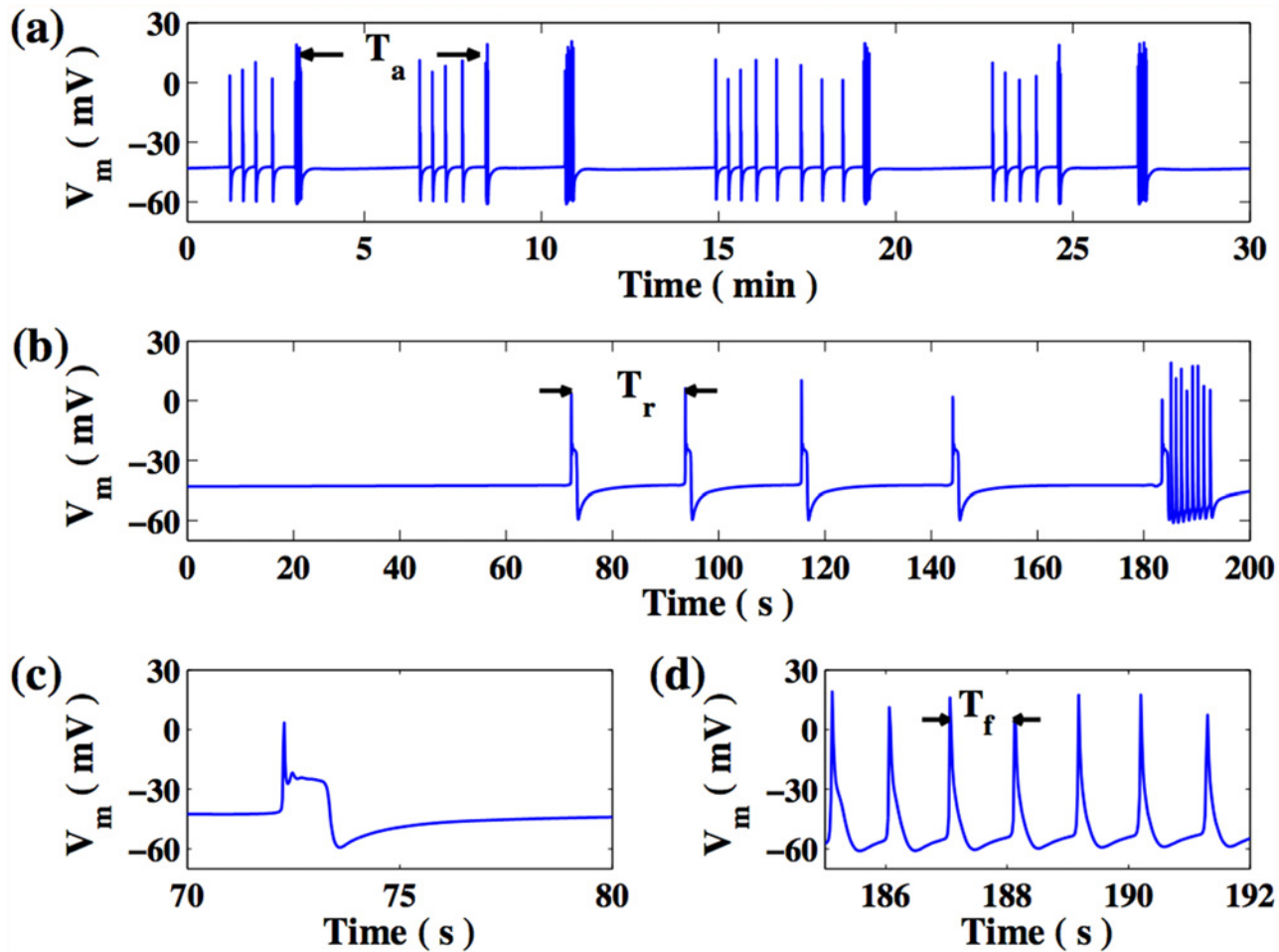
Fig 8. Irregular patterns of activity in the 2-D lattice of coupled myocytes and passive cells. The regime observed here corresponds to an inter-myocyte coupling strength, $G_m = 12nS$. (a) The membrane potential of a single cell exhibits recurrent patterns of activity, each pattern arising after an interval T_a. (b) Each pattern is characterized by an initial quiescent phase, followed by a series of action potentials with period $T_r \sim 20s$ and a brief duration of fast oscillations with periods $T_f \sim 1s$. The profiles of a representative action potential (c) and fast oscillations (d) are also shown.

doi:10.1371/journal.pone.0118443.g008

generic cell in the lattice. The evolution of the membrane potential of a single randomly select-ed cell for $G_m = 12nS$ is shown in Fig. 8. We observe periodically occuring patterns of irregular activity, with consecutive patterns separated by $T_a \sim 4$ min. The structure of this irregular pat-tern is shown in Fig. 8 (b), where a sequence of action potentials with a period $T_r \sim 20s$ are fol-lowed by a set of fast oscillations of period $T_f \sim 1s$. As seen from Fig. 8 (c-d), the fast oscillations do not exhibit the "plateau" that characterizes action potentials. We find that the initial regular activity (of period T_r) arises from waves generated by a single, dominant "pace-maker" region which, as suggested by the detailed analysis of a simplified model [48], is charac-terized by a high density of passive cells.

The irregular behaviour is a consequence of transient, recurrent spiral wave activity (Fig. 9). The motion of the spiral wave can be characterized by the trajectory of its tip, which is defined here as the position on the lattice where the membrane potential is $V_m = -30mV$, intermediate between resting and depolarized states, and where the variable h, describing the inactivation of sodium channels is equal to $h = 0.5$. The motion of the spiral tip over a single rotation period is
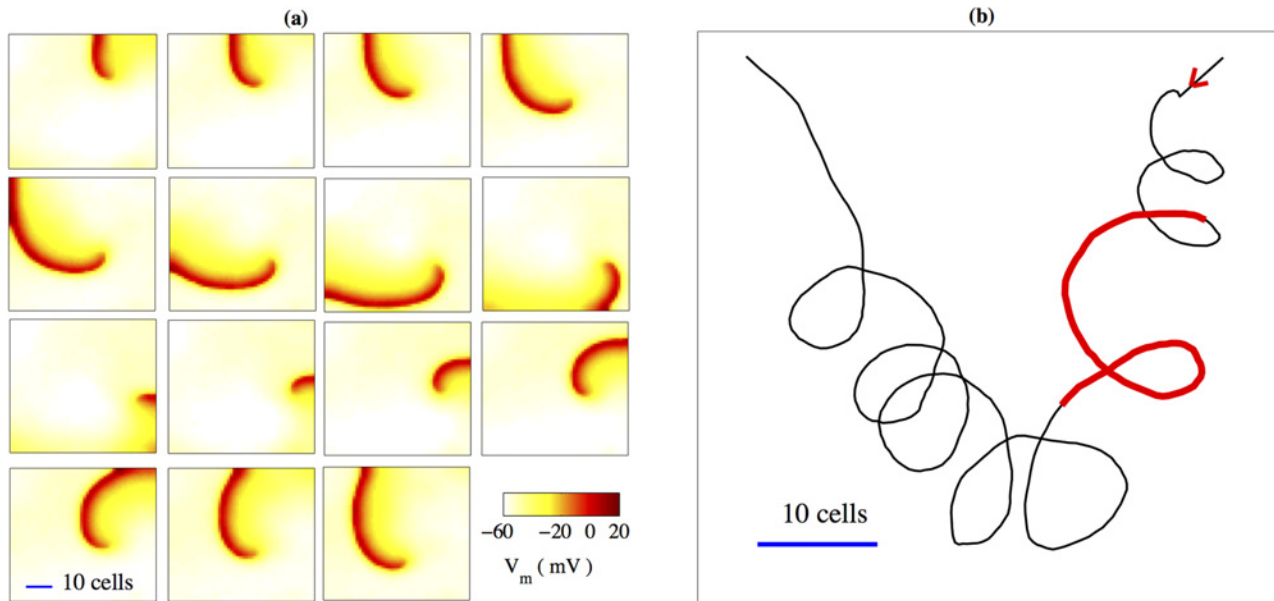
Fig 9. Spiral wave activity. Occurrence of spiral waves of activity in a 50×50 lattice of coupled myocytes and passive cells, observed for inter-myocyte coupling strength, $G_m = 12nS$. (a) Snapshots of membrane potential are shown at intervals of $T = 100ms$, in sequence from left to right and from top to bottom. (b) Trajectory indicating the motion of the tip of the spiral on the 2-D lattice. The two arrows indicate the locations of the spiral when it emerges and disappears, respectively The thick segment corresponds to the sequence shown in (a). The horizontal bars in the lowest, left-most panel of (a), and in (b) indicate the length corresponding to 10 cells, which is of the order of $\sim 1 - 2mm$.

doi:10.1371/journal.pone.0118443.g009

shown in Fig. 9 b. We observe that the emergence of spiral activity is not sensitive to the precise choice of model parameters.

To quantitatively characterize the spiral dynamics, we identify T_f as the rotation period of the spiral and T_a as the interval between two successive appearances of transient spiral activity. Additionally, T_r is identified as the interval between successive regular waves generated by the region with higher passive cell density. We also define N_r as the number of regular waves appearing prior to the appearance of a spiral and N_f as the number of rotations by a spiral during its lifetime. Fig. 8 shows that the values of the characteristic times T_a, T_r and T_f, as well as N_r and N_f, vary between successive irregular patterns. Nevertheless, simulations over large time scales confirm that the behaviour shown in Fig. 8 is statistically stationary. Fig. 10 displays the dependence of the mean of these quantities, obtained over a sufficiently long time interval, on G_m, with the error bars indicating the standard deviation. We observe that the mean value of T_a is approximately constant over the range $6nS \leq G_m \leq 19.2nS$. In contrast, the mean value of T_r (T_f) slightly increases (decreases). Despite the relatively large error bars for N_r and N_s, we find that these quantities remain more or less constant, except for a decrease in N_r at low G_m.

Discussion

In this paper we address the question as to how spontaneous contraction-inducing currents can emerge in the uterus despite the absence of any clearly identifiable pacemaker cells in this organ. Our proposed solution is motivated in part by the experimental observation that gap junction expression strongly increases towards the end of pregnancy [23, 24], leading to an increase in inter-cellular coupling. We investigate the role of such coupling in triggering spontaneous uterine activity by considering the coupling of excitable myocyte cells to electrically passive cells in a mathematical model. We have used a realistic description of myocyte activity
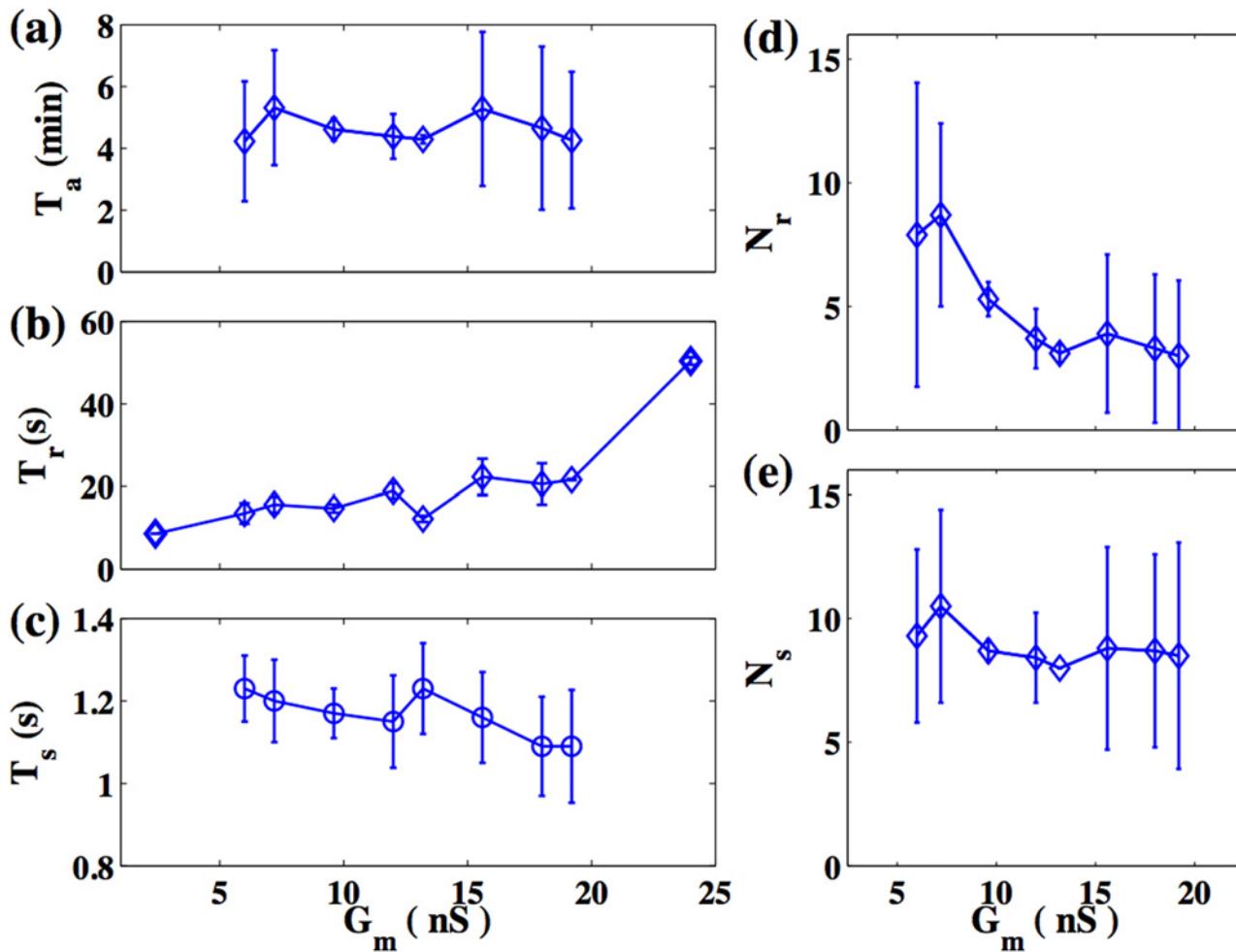
Fig 10. Characterisation of the irregular regimes. Dependence on G_m of the quantities characterizing the patterns of activity shown in Fig. 8, namely the mean values of (a) T_a, (b) T_r, and (c), T_f (c); and of the number of (d) action potentials, N_r, and (e) fast oscillations, N_f. The error bars indicate the standard deviation of the fluctuations of each individual quantity. Each quantity is measured over an interval of at least 6000 s. The quantities shown here have been determiend after averaging over 30 independent realizations of the passive cell distribution.

doi:10.1371/journal.pone.0118443.g010

based on a model recently developed by Tong *et al.* [41], and have incorporated interaction between myocytes and passive cells. We investigate the collective activity of such an assembly both in the context of a single myocyte coupled to one or more passive cells, as well as a 2-D lattice of myocytes with nearest neighbor coupling with each myocyte interacting with a randomly distributed number of passive cells. While simplified models of excitable cells interacting with passive cells have been considered in earlier investigations [36], the use of physiologically realistic model in the present paper allows us to make semi-quantitative predictions and provides a framework for explaining uterine tissue activity both *in vitro* and *in vivo*.

In addition to the gap junctional expression, several other physiological parameters, such as the sodium conductance, g_{Na}, have been observed to change significantly through the course of pregnancy [21]. The experimentally observed values of the resting potential of Interstitial Cajal-like cells (ICLC), as well as of myocytes, are also found to vary over a wide range. For the purposes of our simulations, we choose a set of parameters over a range well within the bounds

set by experimental observations. We have confirmed that the results of our model simulations are qualitatively robust to small variations in parameter values (see SI for details).

We find that the properties of a single myocyte coupled to a number of passive cells are qualitatively very similar to the behaviour observed using a simple excitable model description of myocyte activity [36]. The coupling between myocyte and passive cells, G_p has been chosen to be of the order of $\sim 1nS$, which corresponds to the expression of $\sim$ 20 gap junctions of conductance ~ 50 pS [46]. We note that this is realistic, given the number of gap junctions known to be expressed in a myocyte [24].

We observe that the quantitative nature of our numerical results is dependent on the precise value of the passive cell resting potential, V_p^r, as can be seen from Fig. 3. It has been experimentally observed that the resting potential of an ICLC is -58 ± 7 mV. As the fraction of ICLCs in the tissue does not exceed $n_p \approx 0.2$ [14, 19], the results shown in Fig. 4 suggest that no oscillations would occur in a tissue containing only myocytes and ICLCs. However, uterine tissue contains other electrically passive cells, such as fibroblasts which have a much higher resting potential, $V_p^F \approx -15mV$, and are known to play an important structural role in uterine tissue [16, 17]. A theoretical analysis, documented in the Supplementary Information, suggests that a small population of such passive cells may result in an "effective" resting potential for the passive cells that is higher than that of ICLCs alone. This provides a justification for the range of values of V_p^r used in the simulations reported here, which exhibit spontaneous oscillations in a system of coupled myocytes and passive cells.

For the situation in which myocytes are coupled on a 2-D lattice to their nearest neighbors, as well as to a random number of passive cells, we observe that a progressive increase in the coupling between cells results in a gradual transition from quiescence to the appearance of small clusters of oscillating cells. Further increase in coupling causes these clusters to grow and merge until a single cluster occupies the entire system. These features are qualitatively consistent with observations from experiments on a co-culture of myocytes and fibroblasts [35]. This transition to regular global synchronization occurs via an interesting dynamical regime in which transient, recurrent spiral waves propagate through the system giving rise to activity with a period of $\sim 1s$. This regime of irregular spatiotemporal behaviour has not been previously reported. It is of interest to note that these patterns resemble the complex waves seen in *in vitro* experiments on guinea pig uterine tissue performed by Lammers *et al* [44]. Thus, although a precise quantitative comparison between simulations and experiments would require a more exhaustive investigation, our results are in close qualitative agreement with the observed features of waves propagating in uterine tissue.

We find that it takes approximately $340ms$ for a wave to propagate across a 2-D myocyte assembly of size 50×50 cells. Assuming that the length of a cell is $\sim 225\mu m$ [21], this corresponds to an action potential propagation velocity of $\approx 3.3cm/s$, which is consistent with the values obtained in Ref. [44, 51]. We observe that the period of fast activity is of the order of $\sim 1s$, which is also in agreement with the results of Ref. [44]. Additionally, we note that the value of the inter-myocyte coupling used to obtain the patterns shown in Figs. 8 and 9 is $G_m = 12nS$, which corresponds to an expression of $n_{gj} \approx 240$ gap junctions, a value consistent with experimental observations [24].

For medical applications, the key question is to understand the generation of force in the uterine tissue. In myocytes, action potentials induce a large influx of Calcium, which in turn leads to cell contraction. Available models addressing the question of force generation rest on bursts of Calcium influx inside cells [41, 43, 52]. It is an open question as to whether such activity is a result of intrinsic electrophysiological dynamics of local cell clusters or due to re-entrant waves propagating around the organ. We note that in our simulation of a 2-D lattice of coupled

myocytes and passive cells, rapid spiking activity is observed when the system exhibits spiral waves (Figs. 8 and 9). Determining whether spirals induce transient, pathological contractions, as is the case in the heart, or are required to generate a strong force at the time of delivery, cannot be answered without a better understanding, both at the cellular and tissue level [9, 44].

The results reported in this paper present a picture that is qualitatively, and to an extent quantitatively, consistent with a number of experimental observations, despite the limitations inherent to physiologically detailed models, such as the uncertainties in the characterization of potentially crucial model parameters. This suggests that the mechanism under consideration, namely the electrical coupling between excitable myocytes and passive cells, is at least partially responsible for the generation of spontaneous electrical activity. Our work provides a feasible and falsifiable hypothesis that suggests new avenues for further investigation into this issue, such as the effect of increasing sodium conductance, or the role of hormones such as oxytoxin in the course of pregnancy.

Supporting Information

S1 Table. Parameters used in the model. Values of the parameter used in the description of the Na^+-Ca^{2+} exchanger. The description of the Na^+-Ca^{2+} exchanger in Tong *et al.* [41] was based on the approach of Weber *et al.* [45], and we use the latter values in the current work, with the exception of $K_{m,Allo}$, whose value was chosen to lie between the corresponding values used in Weber *et al.* [45] and that displayed in the SI of Tong *et al.* [41].
(PDF)

S1 Fig. Simulated voltage-clamp experiments on Ca^{2+} channels. (a)-(b) Behaviour of L-type Ca^{2+} channel current, I_{CaL}, for different depolarizing potentials in the range −40 mV to 0 mV at voltage steps of 10 mV with a holding potential $V_h = -60$mV, shown both as a function of (a) time and (b) depolarizing potential V_d, superimposed with results obtained using the model of Tong *et al.* [41]. (c) Behaviour of T-type Ca^{2+} channel current, I_{CaT}, for different depolarizing potentials in the range −60 mV to 20 mV, with a holding potential $V_h = -80$mV.
(TIFF)

S2 Fig. Simulated voltage-clamp experiments on Na^+ and K^+ channels. (a) Behaviour of Na^+ channel current, I_{Na}, at different depolarizing potentials in the range −40 mV to 20 mV with a holding potential $V_h = -40$ mV. (b) Behaviour of the K^+ channel current I_{K1} for $g_k = 0.8nS/pF$, at different depolarizing potentials in the range −40 mV to 10 mV with a holding potential $V_h = -80$ mV, normalized to the peak current at 10 mV. (c) Behaviour of the total K^+ channel current, at different depolarizing potentials in the range −30 mV to 70 mV with a holding potential $V_h = -80$ mV, normalized to the peak current at $V_d = 70$ mV.
(TIFF)

S3 Fig. Simulated action potentials. Action potentials using the model used in this article, compared with the corresponding results obtained using the model of Tong *et al.* [41], for the situations where: (a) A depolarizing current clamp of amplitude $I_{st} = -0.5pA/pF$ is applied for two seconds under control conditions (c.f. Figure 12 of Tong *et al.* [41]). (b) A stimulus of amplitude −1.5 pA/pF is applied over 20 ms at 0.4 Hz (c.f. Figure 13 of Tong *et al.* [41]).
(TIFF)

S4 Fig. Response to a constant stimulus. Behaviour of the model of Tong *et al.* [41], for the situation where a constant stimulus ($I_{st} = -0.1$ pA/pF) is applied for two values of the sodium conductance, viz. (a) $g_{Na} = 0$ nS/pF, and (b) $g_{Na} = 0.04$ nS/pF. The evolution of the [top]

membrane potential, and [bottom] intracellular calcium concentration is displayed in each case. The vertical dashed line indicates the time at which the stimulus is turned off.
(TIFF)

S5 Fig. Response to a constant stimulus after the stimulating current is turned off. Behaviour of our model for the situation where a constant stimulus (I_{st} = -0.1pA/pF) is applied. When the current is turned off (at the time indicated by vertical dashed line), the oscillations cease, and the system eventually returns to its resting state.
(TIFF)

S6 Fig. Decay rates of the coupled system myocyte-passive cell. Decay rates $\lambda_{1,2,3}$ of membrane potentials V_m, V_I and V_F, respectively. When C_m (C_I) is changed by 50%, while leaving C_F and C_I (C_m) unchanged, it can be seen that the fibroblast has the largest decay rate that is one order of magnitude larger than the others. The method is applied to determine the decay rate of the other cells.
(TIFF)

S7 Fig. Eigenvectors corresponding to the relaxation of the system myocyte-passive cell. Components of eigenvectors associated with (a) λ_1, (b) λ_2 and (c) λ_3.
(TIFF)

S8 Fig. Phase space for a coupled system myocyte-passive cell. The (n_p, G_p) parameter space for the case of a single myocyte coupled to n_I ICLCs and n_F fibroblasts, indicating the region where oscillations are observed. The ratio of fibroblasts to ICLCs, $nF{:}nI$ is 1:9. For comparison with the results of coupling a myocyte with an effective passive cell see Fig. 4 in the main text.
(TIFF)

Acknowledgments

Author Contributions

Conceived and designed the experiments: JX SNM RS NBG SS AP. Performed the experiments: JX SNM. Analyzed the data: JX SNM NBG SS AP. Wrote the paper: JX SNM NBG SS AP. Worked on numerical tools: RS NBG.

References

1. Landa JF, West TC, Thiersch JB (1959) Relationships between contraction and membrane electrical activity in the isolated uterus of the pregnant rat. Am J Physiol 196: 905–909. PMID: 13637242

2. Csapo IA, Kuriyama HA (1963) Effects of ions and drugs on cell membrane activity and tension in the postpartum rat myometrium. J Physiol 165: 575–592. doi: 10.1113/jphysiol.1963.sp007081 PMID: 14024103

3. Bengtsson B, Chow EM, Marshall JM (1984) Activity of circular muscle of rat uterus at different times in pregnancy. Am J Physiol Cell Physiol 246: C216–C223.

4. Pervolaraki E, Holden AV (2012) Human uterine excitation patterns leading to labour: Synchronization or propagation? In: Lones MA, Smith SL, Teichmann S, Naef F, Walker JA, Trefzer MA, editors, Lecture Notes in Computer Science, Springer Berlin Heidelberg, volume 7223. pp. 162–176.

5. Martin JA, Kirmeyer S, Osterman MHS, Shepherd RA (2009) Born a bit too early: recent trends in late preterm births. Technical report, Centers for Disease Control and Prevention National Center for Health Statistics 3311 Toledo Road, Hyattsville, Maryland 20782, USA.

6. Norman JE, Morris C, Chalmers J (2009) The effect of changing patterns of obstetric care in Scotland (1980–2004) on rates of preterm birth and its neonatal consequences: Perinatal database study. PLoS Med 6: e1000153. doi: 10.1371/journal.pmed.1000153 PMID: 19771156

7. Mathews TJ, MacDorman MF (2012) Infant mortality statistics from the 2008 period linked birth/infant death data set. National Vital Statistics Reports 60. PMID: 24974588

8. Garfield RE, Maner WL (2007) Physiology and electrical activity of uterine contractions. Semin Cell Dev Biol 18: 289–295. doi: 10.1016/j.semcdb.2007.05.004 PMID: 17659954

9. Lammers WJEP (2013) The electrical activities of the uterus during pregnancy. Reprod Sci 20: 182–189. doi: 10.1177/1933719112446082 PMID: 22649122

10. Sergeant GP, Hollywood MA, McCloskey KD, Thornbury KD, McHale NG (2000) Specialised pacemaking cells in the rabbit urethra. J Physiol 526: 359–366. doi: 10.1111/j.1469-7793.2000.t01-2-00359.x PMID: 10896724

11. McHale N, Hollywood M, Sergeant G, Thornbury K (2006) Origin of spontaneous rhythmicity in smooth muscle. J Physiol 570: 23–28. doi: 10.1113/jphysiol.2005.098376 PMID: 16239271

12. Wray S, Kupittayanant S, Shmygol A, Smith RD, Burdyga T (2001) The physiological basis of uterine contractility: A short review. Exp Physiol 86: 239–246. doi: 10.1113/eph8602114 PMID: 11429640

13. Popescu LM, Faussone-Pellegrini MS (2010) Telocytes—a case of serendipity: the winding way from interstitial cells of cajal (icc), via interstitial cajal-like cells (iclc) to telocytes. J Cell Mol Med 14: 729–740. doi: 10.1111/j.1582-4934.2010.01059.x PMID: 20367664

14. Popescu LM, Ciontea SM, Cretoiu D (2007) Interstitial cajal-like cells in human uterus and fallopian tube. Ann N Y Acad Sci 1101: 139–165. doi: 10.1196/annals.1389.022 PMID: 17360808

15. Popescu LM, Ciontea SM, Cretoiu D, Hinescu ME, Radu E, Ionescu N, et al. (2005) Novel type of interstitial cells (cajal-like) in human fallopian tube. J Cell Mol Med 9: 479–523. doi: 10.1111/j.1582-4934.2005.tb00376.x PMID: 15963270

16. Takemura M, Itoh H, Sagawa N, Yura S, Korita D, Kakui K, et al. (2005) Cyclic mechanical stretch augments hyaluronan production in cultured human uterine cervical fibroblast cells. Mol Hum Reprod 11: 659–665. doi: 10.1093/molehr/gah229 PMID: 16199413

17. Malmström E, Sennström M, Holmberg A, Frielingsdorf H, Eklund E, Malmstöm L, et al. (2007) The importance of fibroblasts in remodelling of the human uterine cervix during pregnancy and parturition. Mol Hum Reprod 13: 333–341. doi: 10.1093/molehr/gal117 PMID: 17337476

18. Parkington HC, Tonta MA, Brennecke SP, Coleman HA (1999) Contractile activity, membrane potential, and cytoplasmic calcium in human uterine smooth muscle in the third trimester of pregnancy and during labor. Am J Obstet Gynecol 181: 1445–1451. doi: 10.1016/S0002-9378(99)70390-X PMID: 10601927

19. Young RC (2007) Myocytes, myometrium, and uterine contractions. Ann N Y Acad Sci 1101: 72–84. doi: 10.1196/annals.1389.038 PMID: 17442780

20. Duquette R, Shmygol A, Vaillant C, Mobasheri A, Pope M, Burdyga T, et al. (2005) Vimentin-positive, c-kit-negative interstitial cells in human and rat uterus: A role in pacemaking? Biol Reprod 72: 276–283. doi: 10.1095/biolreprod.104.033506 PMID: 15385413

21. Yoshino M, Wang S, Kao C (1997) Sodium and calcium inward currents in freshly dissociated smooth myocytes of rat uterus. J Gen Physiol 110: 565–577. doi: 10.1085/jgp.110.5.565 PMID: 9348328

22. Wang S, Yoshino M, Sui J, Wakui M, Kao P, Kao C (1998) Potassium currents in freshly dissociated uterine myocytes from nonpregnant and late-pregnant rats. J Gen Physiol 112: 737–756. doi: 10.1085/jgp.112.6.737 PMID: 9834143

23. Miller SM, Garfield RE, Daniel EE (1989) Improved propagation in myometrium associated with gap junctions during parturition. Am J Physiol Cell Physiol 256: C130–C141.

24. Miyoshi H, Boyle M, MacKay L, Garfield R (1996) Voltage-clamp studies of gap junctions between uterine muscle cells during term and preterm labor. Biophys J 71: 1324–1334. doi: 10.1016/S0006-3495(96)79332-3 PMID: 8874006

25. Döring B, Shynlova O, Tsui P, Eckardt D, Janssen-Bienhold U, Hofmann F, et al. (2006) Ablation of connexin43 in uterine smooth muscle cells of the mouse causes delayed parturition. J Cell Sci 119: 1715–1722. doi: 10.1242/jcs.02892 PMID: 16595547

26. Kirchhoff S, Nelles E, Hagendorff A, Krüger O, Traub O, Wilecke K (1998) Reduced cardiac conduction velocity and predisposition to arrhythmias in connexin40-deficient mice. Current Biology 8: 299–302. doi: 10.1016/S0960-9822(98)70114-9 PMID: 9501070

27. Tsai ML, Cesen-Cummings K, Webb R, Loch-Caruso R (1998) Acute inhibition of spontaneous uterine contractions by an estrogenic polychlorinated biphenyl is associated with disruption of gap junctional communication. Toxicol Appl Pharmacol 152: 18–29. doi: 10.1006/taap.1998.8516 PMID: 9772196

28. Wang CT, Loch-Caruso R (2002) Phospholipase-mediated inhibition of spontaneous oscillatory uterine contractions by lindane in Vitro. Toxicol Appl Pharmacol 182: 136–147. doi: 10.1006/taap.2002.9411 PMID: 12140177

29. Loch-Caruso R, Criswell K, Grindatti C, Brant K (2003) Sustained inhibition of rat myometrial gap junctions and contractions by lindane. Reproductive Biology and Endocrinology 1: 62. doi: 10.1186/1477-7827-1-62 PMID: 14567758

30. Jacquemet V (2006) Pacemaker activity resulting from the coupling with nonexcitable cells. Phys Rev E 74: 011908. doi: 10.1103/PhysRevE.74.011908

31. Kryukov AK, Petrov VS, Averyanova LS, Osipov GV, Chen W, Drugova O, et al. (2008) Synchronization phenomena in mixed media of passive, excitable, and oscillatory cells. Chaos 18: 037129. doi: 10.1063/1.2956985 PMID: 19045503

32. Majumder R, Nayak AR, Pandit R (2012) Nonequilibrium arrhythmic states and transitions in a mathematical model for diffuse fibrosis in human cardiac tissue. PLoS One 7. doi: 10.1371/journal.pone.0045040

33. Bub G, Shrier A, Glass L (2002) Spiral wave generation in heterogeneous excitable media. Phys Rev Lett 88: 058101. doi: 10.1103/PhysRevLett.88.058101 PMID: 11863783

34. Pumir A, Arutunyan A, Krinsky V, Sarvazyan N (2005) Genesis of ectopic waves: Role of coupling, automaticity, and heterogeneity. Biophys J 89: 2332–2349. doi: 10.1529/biophysj.105.061820 PMID: 16055545

35. Chen W, Cheng SC, Avalos E, Drugova O, Osipov G, Lai PY, et al. (2009) Synchronization in growing heterogeneous media. Europhys Lett 86: 18001. doi: 10.1209/0295-5075/86/18001

36. Singh R, Xu J, Garnier NG, Pumir A, Sinha S (2012) Self-organized transition to coherent activity in disordered media. Phys Rev Lett 108: 068102. doi: 10.1103/PhysRevLett.108.068102 PMID: 22401124

37. Kohl P, Camelliti P, Burton FL, Smith GL (2005) Electrical coupling of fibroblasts and myocytes: Relevance for cardiac propagation. J Electrocardiol 38: 45–50. doi: 10.1016/j.jelectrocard.2005.06.096 PMID: 16226073

38. Chilton L, Giles WR, Smith GL (2007) Evidence of intercellular coupling between co-cultured adult rabbit ventricular myocytes and myofibroblasts. J Physiol 583: 225–236. doi: 10.1113/jphysiol.2007.135038 PMID: 17569734

39. Kiseleva I, Kamkin A, Pylaev A, Kondratjev D, Leiterer K, Theres H, et al. (1998) Electrophysiological properties of mechanosensitive atrial fibroblasts from chronic infarcted rat heart. J Mol Cell Cardiol 30: 1083–1093. doi: 10.1006/jmcc.1998.0673 PMID: 9689583

40. Rihana S, Terrien J, Germain G, Marque C (2009) Mathematical modeling of electrical activity of uterine muscle cells. Med Biol Eng Comput 47: 665–675. doi: 10.1007/s11517-009-0433-4 PMID: 19301052

41. Tong WC, Choi CY, Karche S, Holden AV, Zhang H, Taggart MJ (2011) A computational model of the ionic currents, Ca^{2+} dynamics and action potentials underlying contraction of isolated uterine smooth muscle. PLoS ONE 6: e18685. doi: 10.1371/journal.pone.0018685 PMID: 21559514

42. Bursztyn L, Eytan O, Jaffa AJ, Elad D (2007) Modeling myometrial smooth muscle contraction. Ann N Y Acad Sci 1101: 110–138. doi: 10.1196/annals.1389.025 PMID: 17303825

43. Maggio C, Jennings S, Robichaux J, Stapor P, Hyman J (2012) A modified Hai-Murphy model of uterine smooth muscle contraction. Bull Math Biol 74: 143–158. doi: 10.1007/s11538-011-9681-1 PMID: 21882077

44. Lammers WJEP, Mirghani H, Stephen B, Dhanasekaran S, Wahab A, Al Sultan MAH, et al. (2008) Patterns of electrical propagation in the intact pregnant guinea pig uterus. Am J Physiol Regul Integr Comp Physiol 294: R919–R928. doi: 10.1152/ajpregu.00704.2007 PMID: 18046017

45. Weber CR, Ginsburg KS, Philipson KD, Shannon TR, Bers DM (2001) Allosteric regulation of Na/Ca exchange current by cytosolic Ca in intact cardiac myocytes. J Gen Physiol 117: 119–132. doi: 10.1085/jgp.117.2.119 PMID: 11158165

46. Valiunas V, Doronin S, Valiuniene L, Potapova I, Zuckerman J, Walcott B, et al. (2004) Human mesenchymal stem cells make cardiac connexins and form functional gap junctions. J Physiol 555: 617–626. doi: 10.1113/jphysiol.2003.058719 PMID: 14766937

47. Kohl P, Kamkin A, Kiseleva I, Noble D (1994) Mechanosensitive fibroblasts in the sino-atrial node region of rat heart: Interaction with cardiomyocytes and possible role. Exp Physiol 79: 943–1956. doi: 10.1113/expphysiol.1994.sp003819 PMID: 7873162

48. Xu J, Singh R, Garnier NG, Sinha S, Pumir A (2013) Large variability in dynamical transitions in biological systems with quenched disorder. New J Phys 15: 093046. doi: 10.1088/1367-2630/15/9/093046

49. Guckenheimer J, Holmes P (1983) Nonlinear oscillations, dynamical systems and bifurcations of vector fields. Springer, New York.

50. Lammers WJEP (1997) Circulating excitations and re-entry in the pregnant uterus. Pflügers Arch 433: 287–293. PMID: 9064644

51. Lammers WJEP, Stephen B, Hamid R, Harron DWG (1999) The effects of oxytocin on the pattern of electrical propagation in the isolated pregnant uterus of the rat. Pflügers Arch 437: 363–370. PMID: 9914392

52. Burdyga T, Wray S, Noble K (2007) In situ calcium signaling, no calcium sparks detected in rat myometrium. Ann N Y Acad Sci 1101: 85–96. doi: 10.1196/annals.1389.002 PMID: 17303831